Interference in Millimeter-Wave Systems with Directional RTS/CTS Handshake

Zhuoling Chen*, Yi Zhong*✉, *Senior Member, IEEE*, Howard H. Yang†
*School of Electron. Inf. & Commun., Huazhong University of Science and Technology, Wuhan, China
†ZJU-UIUC Institute, Zhejiang University, China

***Abstract*—This paper presents a novel analysis of the directional RTS/CTS handshake mechanism using stochastic geometry, treating its impact as a thinning process in a spatial point process. We introduce unique thinning procedures based on the cosine antenna pattern, offering a more accurate representation of directional transmission in millimeter-wave networks. Through these models, we derive expressions for the intensity of concurrent transmitter processes and the mean interference. Our analysis provides key insights into how mean interference varies with system parameters such as antenna configuration and protection distance. Specifically, numerical results demonstrate that increasing the number of transmit antennas reduces interference, though diminishing returns are observed as the number of antennas grows.**

***Index Terms*—Antenna pattern, directional RTS/CTS mechanism, millimeter wave, stochastic geometry**

I. Introduction

A. Motivation

WLAN standards have evolved into one of the most widely deployed and efficient network access technologies. However, their widespread adoption has also highlighted a significant challenge: the hidden terminal problem. The Request-to-Send/Clear-to-Send (RTS/CTS) handshake mechanism was introduced to mitigate this issue [1]. Unlike traditional CSMA, the RTS/CTS mechanism establishes protection zones around both the transmitter and receiver, effectively reducing interference and enhancing communication reliability.

As wireless networks continue to evolve, sub-6 GHz frequency bands are becoming increasingly congested, presenting a significant challenge in meeting future demand [2]. This scarcity of spectrum has driven researchers and industry experts to explore higher-frequency bands to accommodate growing capacity requirements.

In response, the IEEE has developed standards such as 802.11ad and its successor 802.11ay, both of which operate in the millimeter-wave frequency band [3]. These standards leverage the RTS/CTS mechanism to effectively manage channel access and reduce interference, ensuring high performance even in dense environments [4]. The integration of beamforming in 802.11ad/ay enables directional transmission of mmWave signals [5], giving rise to the directional RTS/CTS mechanism.

This study is driven by the need to better understand the spatial distribution and interference patterns introduced by the directional RTS/CTS mechanism. By analyzing the resulting mean interference, we aim to gain insights into how this mechanism affects network performance. Such an understanding is essential for optimizing the design and operation of future mmWave communication systems, where directional signaling plays a key role in achieving high data rates and supporting dense network environments.

B. Related Works

Several studies have explored mmWave networks and their unique characteristics. In [6], real-world measurements at 28GHz and 73GHz were used to derive spatial statistical models for mmWave channels, providing a realistic assessment of dense urban mmWave deployments. The study shows that mmWave signals are highly sensitive to blockages, leading to significantly different path loss laws for line-of-sight (LOS) and non-line-of-sight (NLOS) scenarios.

To account for the distinct differences between LOS and NLOS conditions, [7] presents analytical results for coverage and rate analysis in mmWave cellular networks, using a flat-top antenna pattern to approximate beamforming patterns. Similarly, [8] applies stochastic geometry to analyze mmWave wireless networks within finite areas, adopting the flat-top antenna pattern. In [9], the performance of two inter-cell interference coordination schemes (PL-ICIC and PG-ICIC) is analyzed for millimeter-wave cellular networks.

While the above studies are based on the flat-top antenna pattern—a tractable but simplified model—they introduce significant discrepancies when evaluating overall network performance. To address this, [10] introduces the sinc and cosine antenna patterns, comparing them with the flat-top model to analyze coverage probability in mmWave networks. Furthermore, [11] adopts the cosine antenna pattern and develops a novel stochastic geometry model comprising two subsystems.

A limitation of the aforementioned works is their reliance on the Poisson point process (PPP), which is accurate for ALOHA-based MAC schemes but not suitable for RTS/CTS mechanism networks. In RTS/CTS networks, the distribution of active transmitters and receivers exhibits a repulsive relationship, which PPP fails to capture.

To model this repulsive distribution, previous studies often employed the Matérn Hard-Core Process (MHCP) [12]–[14]. However, MHCP does not fully capture the RTS/CTS mechanism's characteristics, where protection zones are set around both transmitters and receivers. In [15], a marked point

✉The corresponding author is Yi Zhong (yzhong@hust.edu.cn).

ISBN 978-3-903176-73-7

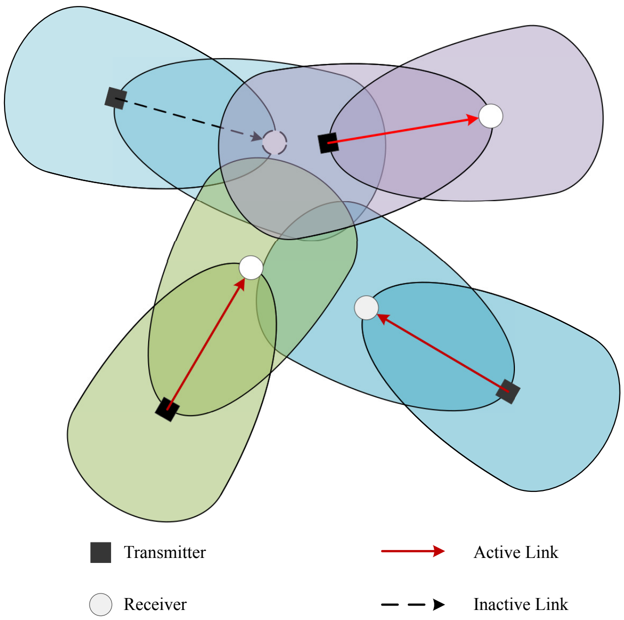

Fig. 1. Illustration of the bipolar model with Type I thinning for the directional RTS/CTS mechanism. In this model, each transmitter (black square) is paired with a corresponding receiver (white circle). The link between the transceiver pair is active only if no other transmitter exists within the combined protection zone.

process model is proposed to more accurately characterize the distribution of transceivers and their corresponding receivers in RTS/CTS networks. However, this model does not account for the directional RTS/CTS mechanism, making it unsuitable for mmWave Wi-Fi systems.

C. Contributions

This paper focuses on the directional RTS/CTS handshake mechanism. The key contributions of our study are summarized as follows:

- We design a protection zone based on the cosine antenna pattern to specifically address the directional transmission characteristics of mmWave signals, as opposed to the traditional disk-shaped protection zone.
- We propose two distinct types of directional thinning, arising from the directional RTS/CTS mechanism in mmWave systems. These thinning effects are fundamentally driven by the unique characteristics of the protection zones. The unique characteristic is expressed through its directionality.
- We derive exact evaluations for the intensity of concurrent transmitter processes and the mean interference, adapting traditional statistical measures to account for the spatial dependencies introduced by the directional RTS/CTS mechanism.

The remainder of this paper is organized as follows: Section II presents the system model, including the protection zones and directional thinning. Section III derives the mean interference for the typical receiver. Section IV verifies the theoretical results through simulations. Finally, Section V concludes the paper.

II. System Model

A. Network and Channel Models

To characterize the locations of transmitters and receivers, we begin with a Poisson bipolar model. All transmitters are assumed to be distributed according to a homogeneous PPP, and have corresponding receivers at the fixed distance D. And we define the effect of directional RTS/CTS as the directional thinning, which selectively keeps some transmitters silent based on the RTS/CTS rule.

All transmitters and receivers are equipped with the uniform liner array (ULA) with N_t antenna elements and N_r antenna elements respectively. The receivers use multiple antennas to feedback CTS after receiving RTS from the corresponding transmitter, and a single antenna for reception, i.e., omnidirectional reception.

After applying the directional RTS/CTS mechanism, transmitters and receivers set up their own protection zone and then transmitters transmit information to the corresponding receivers.

Next we will discuss the channel model. The mmWave propagation environment is characterized by a clustered channel model. In this paper, we focus on the LOS path [10]

$$\mathbf{h}_x = \sqrt{N}\rho_x \mathbf{a}_{\mathrm{t}}^H(\vartheta_x), \tag{1}$$

N is the number of antenna. $\mathbf{a}_{\mathrm{t}}^H(\vartheta_x)$ is the conjugate transpose of the array response vectors. The small-scale fading gain ρ_x follows independent Nakagami-M fading.

B. Directional Thinning

We begin by considering the protection zone of the transmitter. Assume that the transmitters are equipped with uniform linear arrays with N_t antenna elements. The array response vector is expressed as

$$\mathbf{a}_{\mathrm{t}}(\vartheta_x) = \frac{1}{\sqrt{N_{\mathrm{t}}}}\left[1, \cdots, e^{j2\pi k\vartheta_x}, \cdots, e^{j2\pi(N_{\mathrm{t}}-1)\vartheta_x}\right]^T. \tag{2}$$

where $\vartheta_x = \frac{d}{\lambda}\sin\phi_x$, and d, λ, and ϕ_x represent the antenna spacing, wavelength, and physical angle of departure (AoD), respectively.

In the paper, we assume that AoD between each receiver and the corresponding transmitter and is zero. Therefore, the optimal analog beamforming vector for both the transmitter and receiver is

$$\mathbf{w} = \frac{1}{\sqrt{N_{\mathrm{t}}}}\left[1, \cdots, 1, \cdots, 1\right]^T, \tag{3}$$

Using the optimal beamforming vector in (3), the beamforming gain $G_{\mathrm{act}}(\vartheta_x)$ is given by

$$G_{\mathrm{act}}(\vartheta_x) = \left|\mathbf{a}_{\mathrm{t}}^H(\vartheta_x)\mathbf{w}\right|^2 = \frac{\sin^2(\pi N_{\mathrm{t}}\vartheta_x)}{N_{\mathrm{t}}^2\sin^2(\pi\vartheta_x)}. \tag{4}$$

However, the above expression is difficult to analyze further due to the sine functions in both the numerator and denominator. To simplify, we approximate the antenna pattern using the cosine model [10]

$$G_{\cos}(\vartheta_x) = \begin{cases} \cos^2\left(\frac{\pi N_{\mathrm{t}}}{2}\vartheta_x\right) & \text{for } |\vartheta_x| \leq \frac{1}{N_{\mathrm{t}}}, \\ 0 & \text{otherwise.} \end{cases} \tag{5}$$

It is well-known that $\sin x \sim x$ as $x \to 0$. Therefore, we can approximate (5) as

$$G_t(\phi_x) = \begin{cases} \cos^2\left(\frac{\pi N_{\mathrm{t}}\, d}{2\lambda}\phi_x\right) & \text{for } |\phi_x| \le \frac{\lambda}{dN_{\mathrm{t}}}, \\ 0 & \text{otherwise.} \end{cases} \tag{6}$$

We then define the protection zone of transmitter y as S_y

$$S_y = \Big\{ P \in \mathbb{R}^2 : |yP| \le R_t\sqrt{G_t(\phi)}, \quad \cos(\phi) = \frac{\overrightarrow{yP}\cdot\overrightarrow{yx}}{|yP||yx|} \Big\}, \tag{7}$$

where x is the corresponding receiver of transmitter y, and R_t is the maximum protection radius of the transmitter. S_y is the sum of the blue area and the red area in Fig. 2, i.e., the RTS cleaned region.

Similarly, the protection zone of receiver x is defined as

$$S_x = \Big\{ P \in \mathbb{R}^2 : |xP| \le R_r\sqrt{G_r(\phi)}, \quad \cos(\phi) = \frac{\overrightarrow{xP}\cdot\overrightarrow{xy}}{|xP||xy|} \Big\}, \tag{8}$$

where $G_r(\phi)$ is the receiver antenna gain, given by

$$G_r(\phi) = \begin{cases} \cos^2\left(\frac{\pi N_{\mathrm{r}}\, d}{2\lambda}\phi\right) & \text{for } |\phi| \le \frac{\lambda}{dN_{\mathrm{r}}}, \\ 0 & \text{otherwise.} \end{cases} \tag{9}$$

S_x is the sum of the yellow area and the red area in Fig. 2, i.e., the CTS cleaned region.

In the case of omnidirectional antennas, i.e., $d = 0$, $N_t = 1$, and $N_r = 1$, the protection zones S_y and S_x are simply disks centered at y and x, respectively.

1) Type I thinning: We assume $\tilde{\Phi}_a = \{(y_i, \theta_i, k_i)\}$ to be a dependently marked PPP with ground process Φ_a of intensity λ_p on $\mathbb{R}^2$, where

- $\Phi_a = \{y_i\}$ denotes the locations of potential transmitters;
- θ_i denotes the i.i.d. orientation of the receiver for the transmitter y_i, uniformly distributed in $[0, 2\pi]$. Having assumed a constant distance of D between a transmitter and its receiver, the orientation θ_i together with y_i uniquely determines the receiver x_i.
- k_i is the medium access indicator.

For $(y_i, \theta_i, k_i) \in \tilde{\Phi}_a$, let $N(y_i, \theta_i, k_i)$ denotes the number of other transmitters within the protection zone of transceiver pair (y_i, θ_i).

The medium access indicator k_i of (y_i, θ_i, k_i) is a dependent mark defined as

$$k_i = \mathbf{1}(N(y_i, \theta_i) = 0). \tag{10}$$

Thus, type I thinning transforms $\tilde{\Phi}_a$ into

$$\tilde{\Phi} \triangleq \{(x, \theta) : (x, \theta, e) \in \tilde{\Phi}_a, e = 1\}. \tag{11}$$

The intensity of the type I thinning is written as

$$\lambda_b = \lambda_p e^{-\lambda_p S_o}, \tag{12}$$

where S_o is the area of $S_{y_i} \cup S_{x_i}$ and equal to the aggregate area of the red, green, and yellow portions shown in Fig. 2.

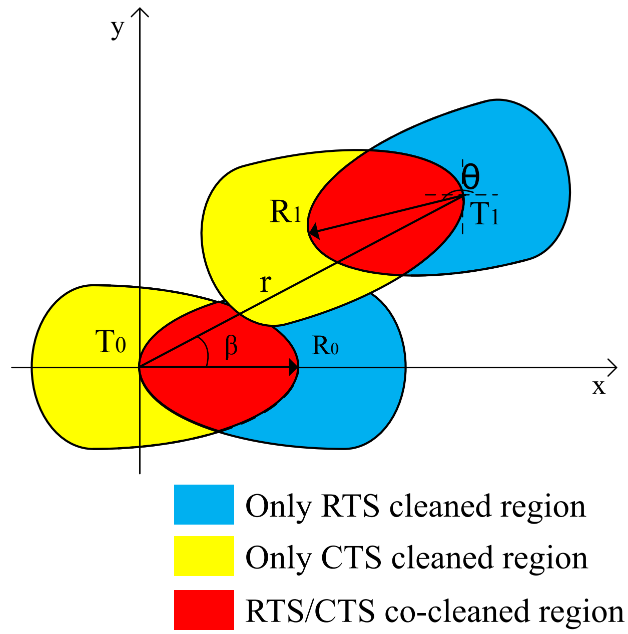

Fig. 2. Illustrative representation of the position relation between the typical transceiver pair and transceiver pair (r, β, θ).

2) Type II thinning: We begin with $\tilde{\Phi}_a = \{(y_i, \theta_i, t_i, k_i)\}$ which is a dependently marked PPP with parent process Φ_a of intensity λ_p on $\mathbb{R}^2$, where

- $\Phi_a = \{y_i\}$ denotes the locations of potential transmitters;
- θ_i denotes the i.i.d. orientation of the receiver for the transmitter y_i, uniformly distributed in $[0, 2\pi]$.
- $\{t_i\}$ are i.i.d. time marks uniformly distributed in $[0, 1]$.
- k_i is the medium access indicator.

For $(y_i, \theta_i, t_i, k_i) \in \tilde{\Phi}_a$, let $N(y_i, \theta_i, t_i)$ denotes the number of special transmitters, which have smaller time marks than t_i and are within the protection zone of transceiver pair (y_i, θ_i).

The medium access indicator k_i of $(y_i, \theta_i, t_i, k_i)$ is a dependent mark defined as

$$k_i = \mathbf{1}(N(y_i, \theta_i, t_i) = 0). \tag{13}$$

Thus, type II thinning transforms $\tilde{\Phi}_a$ into

$$\tilde{\Phi} \triangleq \{(x, \theta) : (x, \theta, t, e) \in \tilde{\Phi}_a, e = 1\}. \tag{14}$$

We get the intensity of the type II thinning as

$$\lambda_b = \frac{1 - e^{-\lambda_p S_o}}{S_o}. \tag{15}$$

III. Mean Interference

In this section, we derive the interference of the directional thinning. Without loss of generality, due to the stationarity of the point process, we focus on the typical transceiver pair with the transmitter y_0 at the origin o and the receiver x_0 at $(D, 0)$, and we condition on $(o, 0) \in \tilde{\Phi}$. And we assume that there is no blockage between typical receiver and any interfering transmitter. Further, we assume that each antenna of transmitters emits the same amount of transmitting power P_0. The total transmitting power, P_t, is the sum of the power from each antenna, i.e., $P_t = P_0 N_t$.

Before derive the mean interference, we introduce the following quantities:

- (r, β, θ) denotes the transceiver pair with the transmitter y at $(rcos(\beta), rsin(\beta))$ and the receiver x at $(r\cos(\beta) + D\cos(\theta), r\sin(\beta) + D\sin(\theta))$. And the typical transceiver pair is $(0, 0, 0)$.
- $S_1 = \{(r, \beta, \theta) : (rcos(\beta), rsin(\beta)) \in S_{y_0} \cup S_{x_0}\}$ denotes the set of the potential transceiver pair (r, β, θ), where the potential transmitter is in the protection zone of the typical transceiver pair. Furthermore, y_0 and x_0 represent the typical transmitter and typical receiver, respectively.
- $S_2 = \{(r, \beta, \theta) : y_0 \in S_y \cup S_x\}$ represents the set of the potential transceiver pair (r, β, θ), where the protection zone contains the typical transmitter. Here, y and x represent the transmitter and receiver, respectively, of the given transceiver pair.
- $G_t(r, \beta, \theta)$ is the approximate array gain of the transmitter of transceiver pair (r, β, θ) to the typical receiver. We employ (6) to express this gain for simplicity. Under condition that the typical transceiver pair is with $\tilde{\Phi}$, (6) depends only on the spatial distribution of interfering transceiver pairs.
- $S(r, \beta, \theta)$ denotes the area of the union of the protection zones of the typical transceiver and the potential transceiver (r, β, θ).

Theorem 1. *The mean interference experienced by the typical receiver x_0 in type I thinning is*

$$E^! (I) = \frac{\lambda_p^2 P_t}{2\pi\lambda_b} \int_0^\infty \int_0^{2\pi} \int_0^{2\pi} l\left(\sqrt{r^2 - 2rD\cos\beta + D^2}\right) G_t(r, \beta, \theta) k(r, \beta, \theta) r\mathrm{d}\theta\mathrm{d}\beta\mathrm{d}r, \tag{16}$$

where $k(r, \beta, \theta)$ is given by

$$k(r, \beta, \theta) = \begin{cases} 0 & (r, \beta, \theta) \in S_1 \cup S_2, \\ \exp\left(-\lambda_p S(r, \beta, \theta)\right) & \textit{otherwise.} \end{cases} \tag{17}$$

Proof. Firstly, we introduce the reduced second order factorial measure of the marked point process $\mathcal{K}_{(r,\beta,\theta)}(B \times L)$ and the transmitter of (r, β, θ) is assumed to be within $\tilde{\Phi}$. And $\lambda\mathcal{K}_{(r,\beta,\theta)}(B \times L)$ is expected number of points located in B with marks taking values in L under the condition of the potential transceiver $(r, \beta, \theta) \in \tilde{\Phi}$.

Using $\mathcal{K}_{(r,\beta,\theta)}(B \times L), B \subset \mathbb{R}^2, L \subset [0, 2\pi]$ [15], we have

$$\begin{aligned} E^!(I) &= E^! \left(\sum_{(x,\theta)\in\tilde{\Phi}} P_0 N_t |\rho_x|^2 l(|x - x_0|) G_t \right) \\ &\overset{(a)}{=} E^! \left(\sum_{(x,\theta)\in\tilde{\Phi}} P_t l(|x - x_0|) G_t \right) \\ &= \lambda P_t \int_{\mathbb{R}^2\times[0,2\pi]} l\left(|x - x_0|\right) \mathrm{G}_t(x, \theta) \mathcal{K}_{(0,0,0)}(\mathrm{d}(x, \theta)), \end{aligned} \tag{18}$$

where (a) follows $|\rho_x|^2$ is distributed according to a gamma distribution $\Gamma(M, \frac{1}{M})$, with the Nakagami parameter M.

The second-order factorial moment measure of the marked point process is written as

$$\begin{aligned} &\alpha^{(2)}(B_1 \times B_2 \times L_1 \times L_2) \\ &= E\left(\sum^{\neq}_{(x_1,\theta_1),(x_2,\theta_2)\in\tilde{\Phi}} 1_{B_1}(x_1) 1_{B_2}(x_2) 1_{L_1}(\theta_1) 1_{L_2}(\theta_2) \right) \\ &= E_{(x_1,\theta_1)\in\tilde{\Phi}} \left(E\left(\sum^{(x_2,\theta_2)\neq(x_1,\theta_1)}_{(x_2,\theta_2)\in\tilde{\Phi}} 1_{B_2}(x_2) 1_{L_2}(\theta_2) \right) \right) \\ &\overset{(a)}{=} \frac{\lambda^2}{2\pi} \int_{B_1\times L_1} \mathcal{K}_{(x,\theta)}((B_2 - x) \times L_2) \mathrm{d}(x, \theta) \\ &\overset{(b)}{=} \int_{B_1\times L_1} \left(\int_{(B_2-x_1)\times L_2} \varrho^{(2)}(x_2, \theta_1, \theta_2) \mathrm{d}(x_2, \theta_2) \right) \mathrm{d}(x_1, \theta_1), \end{aligned} \tag{19}$$

where (a) follows that $E\left(\sum^{(x_2,\theta_2)\neq(x_1,\theta_1)}_{(x_2,\theta_2)\in\tilde{\Phi}} 1_{B_2}(x_2)1_{L_2}(\theta_2)\right)$ is the expected number of points located in B_2 with marks taking values in L_2 under $(x_1, \theta) \in \tilde{\Phi}$, i.e., $\lambda\mathcal{K}_{(x_1,\theta)}((B_2 - x_1)\times L_2)$ and (b) follows the definition of $\alpha^{(2)}$ and the second-order product $\varrho^{(2)}$.

We can derive the relationship between $\mathcal{K}_{(0,0,0)}(B\times L)$ and $\varrho^{(2)}$ as follows:

$$\mathcal{K}_{(0,0,0)}(d(x, \theta)) = \frac{2\pi}{\lambda^2} \varrho^{(2)}(x, 0, \theta)\mathrm{d}(x, \theta). \tag{20}$$

Therefore, (18) can be written as

$$E^!(I_{z_o}) = \frac{2\pi P_t}{\lambda} \int_{\mathbb{R}^2\times[0,2\pi]} l(|x - x_0|)\varrho^{(2)}(x, 0, \theta)G_t(x, \theta)\mathrm{d}(x, \theta). \tag{21}$$

It is clear that the evaluation of $\varrho^{(2)}(x, \theta_0, \theta)$ is

$$\varrho^{(2)}(x, \theta_0, \theta) = \frac{\lambda_p^2}{4\pi^2} k(x, \theta_0, \theta), \tag{22}$$

where $k(x, \theta_0, \theta)$ represents the probability that two transceiver pairs (r_1, β_1, θ_0) with a transmitter y_1 and (r_2, β_2, θ) with a transmitter y_2 are both within $\tilde{\Phi}$ under the condition $|y_1y_2| = x$.

Considering one of the two transceiver pairs is the typical transceiver pair, $k(x, \theta_0, \theta)$ depends only on the location of the other pair, i.e.,

$$E^! (I) = \frac{\lambda_p^2 P_t}{2\pi\lambda_b} \int_0^\infty \int_0^{2\pi} \int_0^{2\pi} l\left(\sqrt{r^2 - 2rD\cos\beta + D^2}\right) G_t(r, \beta, \theta)k(r, \beta, \theta)r\mathrm{d}\theta\mathrm{d}\beta\mathrm{d}r. \tag{23}$$

According to the rule of type I thinning, if the transceiver (r, β, θ) is within $S_1 \cup S_2$, it is impossible that the transceiver and the typical transceiver are both within $\tilde{\Phi}$. And these two pairs are within $\tilde{\Phi}$ if and only if there is no other potential transmitter within the union of the protection zones of two pairs $S(r, \beta, \theta)$. Further, we can get the value of $k(r, \beta, \theta)$ as $\exp(-\lambda_p S(r, \beta, \theta))$ since potential transmitters set Φ_a is a homogenous PPP with intensity λ_p. □

In parallel with Theorem 1, the following theorem gives the mean interference for type II thinning.

Theorem 2. *The mean interference experienced by the typical transceiver pair $y_0(0,0,0)$ in type II thinning is*

$$E^!(I)=\frac{\lambda_p^2P_t}{2\pi\lambda_b}\int_0^{\infty}\int_0^{2\pi}\int_0^{2\pi}$$
$$l\left(\sqrt{r^2-2rD\cos\beta+D^2}\right)G_t(r,\beta,\theta)k(r,\beta,\theta)r\mathrm{d}\theta\mathrm{d}\beta\mathrm{d}r. \tag{24}$$

where $k(r,\beta,\theta)$ is given by

$$k(r,\beta,\theta)=\begin{cases}0 & (r,\beta,\theta)\in S_1\cap S_2,\\ 2p(S) & (r,\beta,\theta)\in\overline{S_1}\cap\overline{S_2},\\ p(S) & \textit{otherwise},\end{cases} \tag{25}$$

in which S is the abbreviation of $S(r,\beta,\theta)$, and $p(S)$ is

$$p(S)=\frac{S_oe^{-\lambda_pS}-Se^{-\lambda_pS_o}+S-S_o}{\lambda_p^2(S-S_o)SS_o}. \tag{26}$$

Proof. The derivation of type II thinning is the same as that of the type I thinning in Theorem 1 except $k(r,\beta,\theta)$.

Let their time marks be t_0 of the typical transceiver and t_2 of the considering transceiver (r,β,θ) respectively. According to the rule of type II thinning, if the transceiver is within $S_1\cap S_2$, it is impossible that the transceiver and the typical transceiver are both retained within $\tilde{\Phi}$. When the transceiver is within $\overline{S_1}\cap\overline{S_2}$, there are two cases of $t_0>t_1$ and $t_0\le t_1$, where pairs can be both retained. Considering the two cases, we can get

$$\begin{aligned}k(r,\beta,\theta)&=\int_0^1 e^{-\lambda_pt_1S_o}\left[\int_0^{t_1}e^{-\lambda_pt_2(S-S_o)}\mathrm{d}t_2\right]\mathrm{d}t_1\\&+\int_0^1 e^{-\lambda_pt_2S_o}\left[\int_0^{t_2}e^{-\lambda_pt_1(S-S_o)}\mathrm{d}t_1\right]\mathrm{d}t_2\\&=\quad 2\int_0^1 e^{-\lambda_pt_1S_o}\left[\int_0^{t_1}e^{-\lambda_pt_2(S-S_o)}\mathrm{d}t_2\right]\mathrm{d}t_1,\end{aligned} \tag{27}$$

which is written as $2p(S)$. If the transceiver is neither within $S_1\cap S_2$ nor within $\overline{S_1}\cap\overline{S_2}$, $k(r,\beta,\theta)=p(S)$. □

IV. Numerical Results

The numerical results are obtained from the analytical results we have derived. The maximum protection distance of transmitters R_t is always set as $R_t=1.2R_r$ and the distance between transmitter and receiver is set as $D=0.8R_r$. The path-loss function is $l(r)=\frac{A}{1+r^{\alpha}}$ with $\alpha=2.1$. To facilitate the comparison of the impact of the number of antennas, we assume $P_tA=1$ and the unit of P_t is milliwatts (mW).

Fig. 3 displays the mean interference of the type I as a function of λ_p. From the curves, we observe that all curves first increases with λ_p and then decreases. This behavior stems from the fact that the intensity of the type I depends on the intensity of ground process λ_p and the thinning probability of a point that decreases with λ_p. In the initial phase, as λ_p increases, the intensity increases due to its direct dependence on the ground process. However, beyond a certain critical point $\frac{1}{S_0}$, the thinning probability begins to dominate the system behavior. Reducing both N_t and N_r will expand the protected area, but reducing N_t actually increases the mean interference with smaller λ_p, shown in Fig. 3, which might seem counterintuitive. This is because increasing N_t results in more transmitters causing interference to the typical receiver. And we observe that the maximum value of the average interference is affected by antenna element and R_r. It is positively correlated with N_t and inversely correlated with R_r and N_r. When λ_p is relatively low, a higher N_t results in fewer active transmitters causing interference to the typical receiver. However, as λ_p increases, a higher N_t leads to a slower decrease in the density of active transmitters with increasing λ_p. This explains why the curves for configurations with higher values of N_t have a gentler slope and the mean interference for high N_t is initially lower than for low N_t, but eventually becomes higher as λ_p increases.

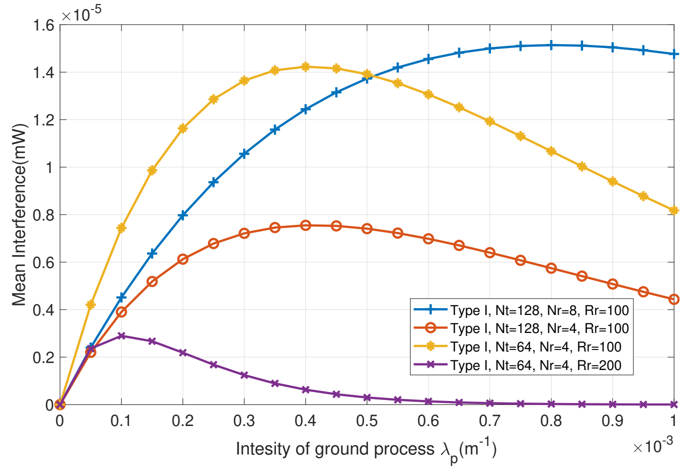

Fig. 3. The mean interference of type I as a function of the intensity of Φ_a.

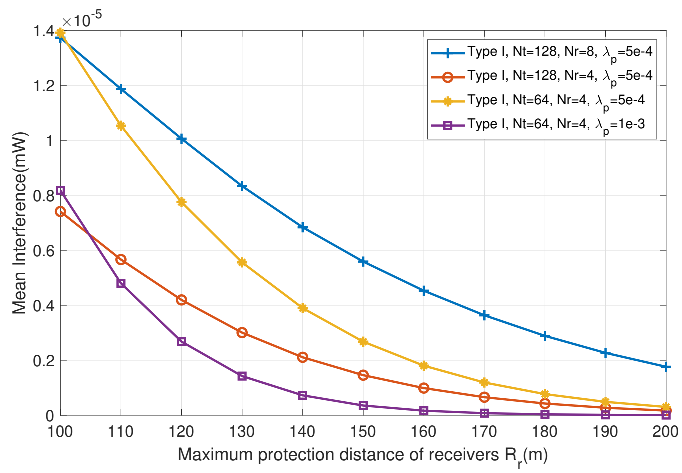

Fig. 4. The mean interference of type I as a function of the maximum protection distance of receiver R_r.

Fig. 4 displays the mean interference of the type I as a function of R_r. As evident from the graph, the mean interference decreases as R_r increases, suggesting that as the protection distance increases, the system experiences a reduction in interference levels. This behavior can be explained by the fact that increasing R_r while maintaining the antennas elements results in a larger protected area. The expansion of the protected region reduces the density of active transmitters,

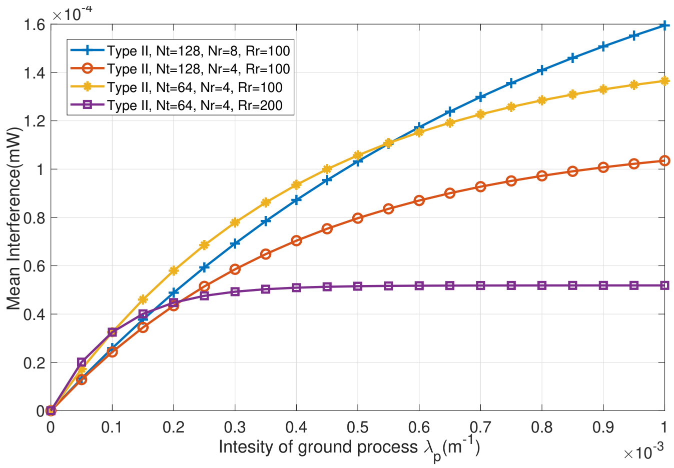

Fig. 5. The mean interference of type II as a function of the intensity of Φ_a.

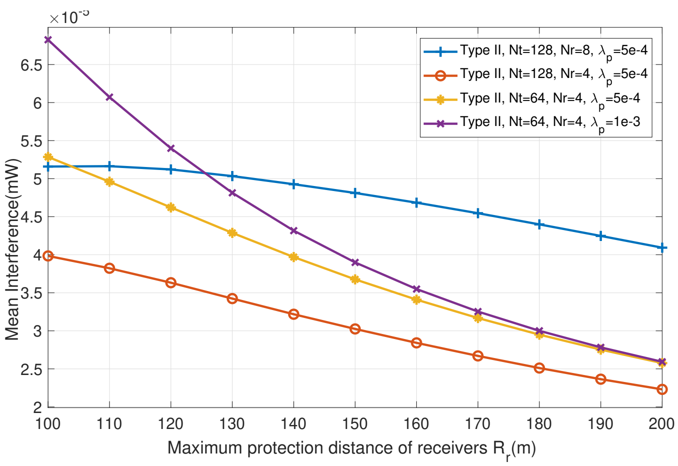

Fig. 6. The mean interference of type II as a function of the maximum protection distance of receiver R_r.

which directly leads to a reduction in interference. This figure illustrates that the curves for configurations with higher N_t values have a gentler slope, aligning with the observations in Fig. 3, indicating that systems for type I with higher N_t values exhibit a more gradual decrease in mean interference as R_r increases. This behavior comes from the same underlying mechanism that causes configurations with higher N_t values to exhibit gentler slopes in their performance curves shown in Fig. 3.

Fig. 5 shows the mean interference of the type II as a function of λ_p. As observed from the graph, the mean interference increases as λ_p rises, suggesting that a higher intensity of the ground process leads to a greater level of interference. However, the rate of this increase diminishes with higher values of λ_p, which indicates that the interference tends to stabilize and approach a constant value as λ_p becomes very large (i.e., as $\lambda_p \to \infty$). This trend can be attributed to the intensity of type II. In the initial phase, the intensity grows with increasing λ_p increases, following the same trend as type I. However, once the density is large enough, the intensity saturates and stabilizes at a constant level. The

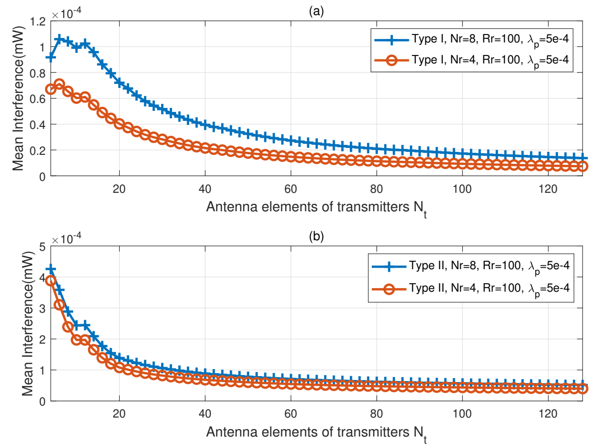

Fig. 7. The mean interference as a function of N_t.

saturation behavior of the mean interference implies that there is an upper bound for the mean interference, beyond which further increases in λ_p will no longer significantly affect the interference. This stable value is influenced by several key factors, including the number of antenna elements, including N_t and N_r, and the maximum protection distance R_r. More specifically, we observe that the stable value is positively correlated with N_t and inversely correlated with R_r and N_r. This is because increasing R_r and N_r will reduce the density of active transmitters, which is the opposite of increasing N_t. Another important observation from the graph is the difference in the slopes of the curves. Similar to type I, the curves for configurations with higher N_t values also exhibit a gentler slope that for low N_t.

Fig. 6 displays the mean interference of the type II as a function of R_r. It is evident from the plot that as R_r increases, the mean interference steadily decreases. From the curves, we observe that curves with the same N_t and N_r will coincide as R_r increases. This behavior implies that the effect of varying λ_p on mean interference becomes less pronounced as the protection distance increases. Furthermore, the curves representing configurations with higher N_t values display a more gradual slope compared to those with lower values N_t. This observation suggests that systems with a higher N_t exhibit greater robustness in terms of their interference performance as the maximum protection distance R_r changes. In other words, the systems with higher N_t values are less sensitive to fluctuations in interference levels, providing a more stable performance across varying distances.

Fig. 7 displays the mean interference as a function of N_t. In (a), the mean interference might fluctuate in the range of smaller N_t values, rather than simply decreasing monotonically as N_t increases. As N_t continues to increase, the mean interference would monotonically decrease and then gradually stabilize. In (b), the mean interference decreases as the number of antenna elements increases overall. And as N_t continues to increase, the mean interference will gradually stabilize, similar to the behavior observed in (a). In both (a) and (b), we observe that the mean interference will trend to stabilize when $N_t \gg N_r$ and N_r only influences the stable value of the mean interference, not the overall trend of it.

V. Conclusion

In this paper, we proposed marked point process models to characterize the spatial distribution of transceivers under the directional RTS/CTS handshake mechanism. We derive the evaluation of the mean interference of a typical receiver and explore how the mean interference varies with system parameters such as the maximum protection distance, the density of transceiver nodes and the number of antennas. Our analysis reveals the impact of increasing the number of transmitting antennas on system interference. Increasing antenna elements can increase robustness of system, but it also leads to higher costs and a high probability of greater interference. Therefore, the design of future millimeter-wave systems must carefully balance these trade-offs to achieve optimal performance and cost efficiency.

VI. Acknowledgement

This research was supported by the National Natural Science Foundation of China (NSFC) under grant No. 62471193, and in part by the Wuhan Science and Technology Program (No. 2024030803010178).

References

[1] F. Tobagi and L. Kleinrock, "Packet Switching in Radio Channels: Part II - The Hidden Terminal Problem in Carrier Sense Multiple-Access and the Busy-Tone Solution," in IEEE Transactions on Communications, vol. 23, no. 12, pp. 1417-1433, December 1975.

[2] M. N. Kulkarni, S. Singh and J. G. Andrews, "Coverage and rate trends in dense urban mmWave cellular networks," 2014 IEEE Global Communications Conference, Austin, TX, USA, 2014.

[3] S. Mohebi, M. Lecci, A. Zanella and M. Zorzi, "The challenges of Scheduling and Resource Allocation in IEEE 802.11ad/ay," 2020 Mediterranean Communication and Computer Networking Conference (MedComNet), Arona, Italy, 2020, pp. 1-4.

[4] "IEEE Standard for Information Technology–Telecommunications and Information Exchange between Systems Local and Metropolitan Area Networks–Specific Requirements Part 11: Wireless LAN Medium Access Control (MAC) and Physical Layer (PHY) Specifications Amendment 2: Enhanced Throughput for Operation in License-exempt Bands above 45 GHz," in IEEE Std 802.11ay-2021 (Amendment to IEEE Std 802.11-2020 as amendment by IEEE Std 802.11ax-2021) , vol., no., pp.1-768, 28 July 2021

[5] X. Wang et al., "Millimeter Wave Communication: A Comprehensive Survey," in IEEE Communications Surveys & Tutorials, vol. 20, no. 3, pp. 1616-1653, third quarter 2018.

[6] M. R. Akdeniz et al., "Millimeter Wave Channel Modeling and Cellular Capacity Evaluation," in IEEE Journal on Selected Areas in Communications, vol. 32, no. 6, pp. 1164-1179, June 2014.

[7] T. Bai and R. W. Heath, "Coverage and Rate Analysis for Millimeter-Wave Cellular Networks," in IEEE Transactions on Wireless Communications, vol. 14, no. 2, pp. 1100-1114, Feb. 2015.

[8] S. M. Azimi-Abarghouyi, B. Makki, M. Nasiri-Kenari and T. Svensson, "Stochastic Geometry Modeling and Analysis of Finite Millimeter Wave Wireless Networks," in IEEE Transactions on Vehicular Technology, vol. 68, no. 2, pp. 1378-1393, Feb. 2019.

[9] H. Wei, N. Deng and M. Haenggi, "Performance Analysis of Inter-Cell Interference Coordination in mm-Wave Cellular Networks," in IEEE Transactions on Wireless Communications, vol. 21, no. 2, pp. 726-738, Feb. 2022.

[10] X. Yu, J. Zhang, M. Haenggi and K. B. Letaief, "Coverage Analysis for Millimeter Wave Networks: The Impact of Directional Antenna Arrays," in IEEE Journal on Selected Areas in Communications, vol. 35, no. 7, pp. 1498-1512, July 2017.

[11] Y. Nabil, H. ElSawy, S. Al–Dharrab, H. Attia and H. Mostafa, "A Stochastic Geometry Analysis for Joint Radar Communication System in Millimeter-wave Band," ICC 2023 - IEEE International Conference on Communications, Rome, Italy, 2023, pp. 5849-5854.

[12] Z. Chen and Y. Zhong, "Characterizing Stability Regions in Wireless Networks With Hard-Core Spatial Constraints," in IEEE Wireless Communications Letters, vol. 13, no. 8, pp. 2180-2184, Aug. 2024.

[13] J. Lyu and H. -M. Wang, "Secure UAV Random Networks With Minimum Safety Distance," in IEEE Transactions on Vehicular Technology, vol. 70, no. 3, pp. 2856-2861, March 2021.

[14] Y. Zhong, Z. Chen, T. Han and X. Ge, "Spatio-Temporal Interference Correlation: Influence of Deployment Patterns and Traffic Dynamics," in IEEE Transactions on Communications, in press, 2025.

[15] Y. Zhong, Z. Chen, W. Zhang, M. Haenggi, "Dual-Zone Hard-Core Model for RTS/CTS Handshake Analysis in WLANs," in arXiv preprint arXiv:2412.09953, 2024.

[16] M. Akdeniz, Y. Liu, M. Samimi, S. Sun, S. Rangan, T. Rappaport, and E. Erkip, "Millimeter wave channel modeling and cellular capacity evaluation," IEEE J. Sel. Areas Commun., vol. 32, no. 6, pp. 1164–1179, Jun. 2014.